Title

High-sensitivity plasma density retrieval in a common-path second-harmonic interferometer through simultaneous group and phase velocity measurement

Journal

Physics of Plasmas, 26(2)

ISSN

1070-664X

Authors

Van Tilborg, J
Gonsalves, AJ
Esarey, E
et al.

Publication Date

2019-02-01

DOI

10.1063/1.5080269

Peer reviewed

High-sensitivity plasma density retrieval in a common-path two-color interferometer through simultaneous group and phase velocity measurement

J. van Tilborg,[1,*] A. J. Gonsalves,[1] E. H. Esarey,[1] C. B. Schroeder,[1] and W. P. Leemans[1]

[1] *Lawrence Berkeley National Laboratory, University of California, Berkeley, California 94720, USA*

(Dated: January 9, 2019)

Precise measurements of the plasma density in ionized gas cells and discharged capillaries are critical to design and operation of plasma-based accelerators, active plasma lenses, and plasma-based radiation sources. In this manuscript, the spectral-domain common-path non-linear interferometer is upgraded with simultaneous measurement of the group and phase velocity, allowing for high-sensitivity density characterization (from the phase velocity advance) without need of phase tracking from zero-density (enabled by the group velocity delay). The technique is applied to 1.5-cm-long plasma structures, without density ambiguity in parameter scans with $> 2\pi$ phase jumps. The single-shot sensitivity in phase retrieval is demonstrated at 63 mrad, equivalent to a density-length product of $1.8 \cdot 10^{15}$ cm^{-2}. This is an improvement of $\times 45$ compared to group velocity analysis alone.

Plasma cells have found applications in plasma-based accelerators (both laser-driven and beam-driven wakefield acceleration [1–4]), as compact ion and electron beam focusing elements [5, 6], and as laser-based radiation sources [7, 8] . Typically, the cm-scale plasma targets are prepared (ionized) with electric discharge pulses or laser pre-pulses, leading to densities in the 10^{15}-10^{19} cm^{-3} range. Radial temperature gradients can lead to the formation of guiding channels with an on-axis density minimum [9–12]. Knowledge of the plasma density is of critical importance to these applications since the density dominates the plasma response time, self-injection threshold, accelerating field strength, electron beam dephasing length [1], beam-driven wakefield effects [13], and radiation-generating phase matching conditions [8]. For example, in laser-plasma accelerators (LPAs), it is well understood from dephasing considerations that the path towards multi-GeV electron energies is to move from mm-long $\sim 10^{18}$ cm^{-3} gas jet plasmas to multi-cm-long $\sim 10^{16} - 10^{17}$ cm^{-3} plasma channels [1].

The plasma structures in the afore-mentioned applications typically are of circular cross-section at diameters on the (sub) mm scale, and multiple cm in length. Transverse spatial-domain interferometry is challenging due to the short transverse cross-section, compounded by the circular capillary body and radial channel profile [14]. Longitudinal spatial-domain interferometry [9] is similarly hindered by the narrow diameter and wavefront evolution in the channel. Recently, Ref. 15 demonstrated a diagnostic solution by performing spectral-domain longitudinal interferometry to retrieve the line-integrated on-axis plasma density. The concept here was to measure the pulse envelope slippage in the plasma due to the density-dependent group velocity reduction. The common-path non-linear geometry was applied to significantly improve the alignment robustness and retrieval accuracy with respect to earlier two-path linear interferometric geometries [16, 17]. Although the intrinsic diagnostic sensitivity (defined as the standard deviation on the pulse slippage measurements with the plasma structure removed, expressed as an equivalent density-length product) was shown to be as low as $8.2 \cdot 10^{16}$ cm^{-2}, it will be presented in this manuscript that this sensitivity is improved to $1.8 \cdot 10^{15}$ cm^{-2} by complimenting the group velocity measurement with simultaneous phase velocity recording.

Phase retrieval in a common-path non-linear geometry has already been demonstrated on gases and plasmas [18–25], and on reflective structures [26]. For example, Ref. 24 presented a diagnostic sensitivity equivalent to a density-length product of $7 \cdot 10^{13}$ cm^{-2}, implemented on the Large Helical Device plasma. Besides the picosecond time resolution, our work differs from previous efforts in two key points. (1) By analyzing the spectral-domain interference by two femtosecond probe beams, as opposed to spatial interference, narrow plasma channels are no longer excluded from diagnostic application. Also, the complexity in the setup is reduced since temporal overlap is not required (the delay between the two pulses can be arbitrary). (2) The broad-bandwidth spectral-domain approach allows for simultaneous group velocity (periodicity of the spectral fringes) and phase velocity retrieval (phase of the fringes). This enables single-shot high-sensitivity phase-based density retrieval without need for phase tracking, since the lesser-sensitive group-velocity retrieval can determine which integer multiple of 2π is applicable to the retrieved phase. Applications where phase-tracking from zero-density is not possible, or parameter scans with phase jumps more than 2π, are thus now accessible with this novel approach. Note that since Ref. 26 also diagnosed spectral-domain fringes on broad-bandwidth pulses (not on plasmas however, but on a reflective metal-oxide semiconductor), the first point (1) of difference does not apply for this reference.

The basic concept is depicted in Fig. 1(a), with a single femtosecond laser pulse traveling through frequency-doubling crystal BBO-1, thus transforming into two co-propagating pulses (a "blue pulse 1" at λ =400 nm and a "red pulse 2" at λ =800 nm). These two pulses are

* JvanTilborg@lbl.gov

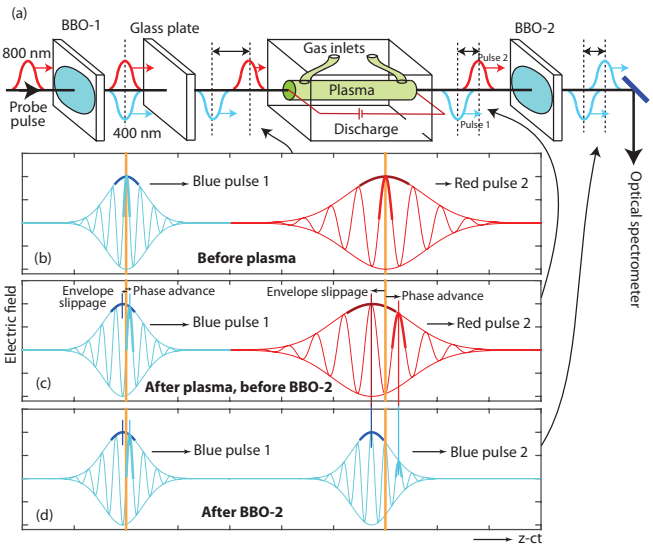

FIG. 1. (color online) (a) Schematic of common-path concept: a fraction of an incoming probe pulse is frequency-doubled in crystal BBO-1 such that two pulses of different color ("blue pulse 1" at λ =400 nm and "red pulse 2" at λ =800 nm) propagate through the plasma. The red pulse experiences a stronger group-velocity-related envelope slippage and phase-velocity-related phase advance when compared to the trailing blue pulse. This is illustrated when comparing the pre-plasma cartoon of the electric field profiles in (b) to the post-plasma situation in (c). The relative envelope slippage and phase advance are conserved after the leading red pulse is doubled to blue by the post-plasma doubling crystal BBO-2. Originating from one input pulse, the two pulses experience one identical path (no de-coupled mirror reflections), thus strongly benefitting stability and diagnostic sensitivity.

intrinsically coupled and locked in timing, phase, pointing, and stability, since they experience the same (common) optical path. Following propagation through the plasma, the two pulses build up a phase and envelope shift due to their carrier frequency difference. A second crystal then doubles the fundamental pulse 2 to its second harmonic "blue pulse 2". Finally, a single-shot spectrum is recorded, delivering the broad-bandwidth modulated spectrum from which both the plasma phase velocity (phase of the spectral fringes) and group velocity (spacing of the spectral fringes) can be retrieved.

The two blue pulses incident on the optical spectrometer share the same power spectrum $I_{\rm env}(\omega)$, with $\omega = 2\pi c/\lambda$ the angular frequency, but each at different accumulated spectral phase $\phi_1(\omega)$ (for pulse 1, already "blue" during plasma propagation) and $\phi_2(\omega)$ (for pulse 2, doubled to "blue" after the plasma). The sum field can be expressed as $E(\omega) = \sqrt{I_{\rm env}(\omega)}\left[e^{i\phi_1(\omega)} + e^{i\phi_2(\omega)}\right]$. The spectral phase accumulated by a plasma of index of refraction $\eta_{\rm plasma}(\omega)$ and length $L_{\rm plasma}$ is

$$\phi_{\rm plasma}(\omega) = (\omega/c)\eta_{\rm plasma}(\omega)L_{\rm plasma}. \qquad (1)$$

At plasma frequency ω_p, with ω_p [s^{-1}] $= 5.64 \cdot 10^4 \times \sqrt{\rm n\ [cm^{-3}]}$ and density n, the plasma index of refraction is $\eta_{\rm plasma}(\omega) = 1 - \omega_p^2/(2\omega^2)$. Thus

$$\phi_1(\omega) = \Phi + \phi_{\rm plasma}(\omega), \qquad (2)$$

with Φ a constant phase-offset linked to the carrier phase of the input red pulse (before BBO-1). Similarly, the phase term for blue pulse 2 can be expressed as

$$\phi_2(\omega) = \Phi + \phi_{\rm mat} + \frac{L_{\rm mat}}{c}\omega + 2\phi_{\rm plasma}(\omega/2). \qquad (3)$$

This expression can be understood as follows: the field at frequency ω first propagated through the plasma at its half-frequency $(\omega/2)$, thus accumulating the phase $\phi_{\rm plasma}(\omega/2)$. In the doubling crystal BBO-2, both the frequency and phase are doubled. The extra term $(\phi_{\rm mat} + \omega L_{\rm mat}/c)$ reflects the "material-related" carrier phase difference ϕ_{mat} and optical path difference $L_{\rm mat}$ accumulated by pulse 2 (propagating through BBO-1 and the glass plate as red, and then doubling to blue in BBO-2) with respect to pulse 1 (doubling to blue in BBO-1 and then propagating through the glass plate and BBO-2). This term is a constant of the setup, with $L_{\rm mat}$ of negative value. The spectrum $I(\omega) = |E(\omega)|^2$ can be written in terms of the phase difference $\Delta\phi(\omega) = \phi_1(\omega) - \phi_2(\omega)$ as

$$I(\omega)/I_{\rm env}(\omega) = \left|1 + e^{i\Delta\phi(\omega)}\right|^2 = 2 + 2\cos\left[\Delta\phi(\omega)\right]. \qquad (4)$$

Inserting Eqs. (2) and (3) in Eq. (4), and applying the Taylor expansion $[1/\omega] \simeq [1/\omega_0] - [(\omega-\omega_0)/\omega_0^2]$ around the central "blue" frequency ω_0, it can be shown that the spectrally-modulated $I(\omega)$ can be expressed as a modulation phase $\phi_{\rm mod}$ and a pulse separation $L_{\rm sep}$ through

$$I(\omega)/I_{\rm env}(\omega) = 2 + 2\cos\left[\phi_{\rm mod} + \frac{L_{\rm sep}}{c} \times (\omega - \omega_0)\right], \qquad (5)$$

with

$$\phi_{\rm mod} = \phi_{\rm mat} + \frac{3}{2}\frac{L_{\rm plasma}}{c}\frac{\omega_p^2}{\omega_0}, \qquad (6)$$

and

$$L_{\rm sep} = L_{\rm mat} - \frac{3}{2}L_{\rm plasma}\frac{\omega_p^2}{\omega_0^2}. \qquad (7)$$

Note that $\Delta\phi(\omega)$ and Eqs. (5)-(7) no longer contain a Φ dependency. The constants $\phi_{\rm mat}$ and $L_{\rm mat}$ can be measured by operating the structure at zero-density. Normalizing $(\phi_{\rm mod} - \phi_{\rm mat})$ into a length unit through $\Delta z_\phi = (\lambda_0/2\pi)(\phi_{\rm mod} - \phi_{\rm mat})$, with $\lambda_0 = 2\pi c/\omega_0$, and expressing $\Delta z_{\rm gr} = (L_{\rm sep} - L_{\rm mat})$, yields

$$\Delta z_\phi = \frac{3}{2}\frac{\omega_p^2}{\omega_0^2}L_{\rm plasma} \quad \text{and} \quad \Delta z_{\rm gr} = -\frac{3}{2}\frac{\omega_p^2}{\omega_0^2}L_{\rm plasma}. \qquad (8)$$

Equation (8) reflects that the linear response of a laser propagating in a plasma requires the product of the group

and phase velocity to be unity. Simultaneous measurement of Δz_ϕ and $\Delta z_{\rm gr}$ allows for high-sensitivity density-length product measurement without the need for phase-tracking from zero-density. For consistency to previous work, the envelope slippage expression in Eq. (3) of Ref. 15 was written in terms of the "red" driver frequency ω_r, and is consistent with Eq. (8) presented here using the conversion $\omega_0 = 2\omega_r$.

Note that for a parabolic density channel, the laser not only probes the on-axis density n_0 but also the higher off-axis densities. To account for this effect when measuring the on-axis group and phase velocity at the capillary exit (as in this manuscript), the radial channel profile as well as the longitudinally-varying beam size evolution for both red and blue beams need to be considered [27]. For a given n_0, matched channel radius r_m, and capillary entrance beam size r_i, one should apply the line-averaged index of refraction $\eta_{\rm plasma}(\omega)$ to Eqs. (2) and (3). Although a negligible effect for the data presented in this manuscript, in general this is accomplished by writing $\eta_{\rm plasma}(\omega) = c/v_\phi(\omega) = \overline{v_{\rm gr}(\omega)}/c$, where $\overline{v_{\rm gr}(\omega)} = (1/L_{\rm plasma}) \int_0^{L_{\rm plasma}} v_{\rm gr}(\omega, r_i, r_m, n_0, z) dz$ with $v_{\rm gr}(\omega, r_i, r_m, n_0, z)$ expressed by Eq. (2) in Ref. 15.

For an experimental demonstration, the setup depicted in Fig. 1(a), and extensively discussed in Ref. 15, was developed. A weak laser pulse (several μJ's, 45 fs duration) was incident on a type-I frequency-doubling BBO crystal (thickness 0.1 mm, diameter 10 mm) and a piece of 1-mm-thick glass to provide a constant temporal offset of order $L_{\rm mat}/c = 250$ fs (blue trailing the red pulse). Then, both pulses entered a H_2-filled capillary of $L_{\rm plasma}$=1.5 cm length and 0.25 mm in diameter. The discharge current pulse, see Fig. 3(c) at peak current of 350 A, was measured for each shot. For the probe laser, beam sizes at the capillary entrance of 71 μm (red pulse) and 47 μm (blue pulse) were measured. After the capillary, the two pulses were routed to a second type-I BBO crystal and onto a spectrometer at 0.8 nm resolution. A typical single-shot interferogram is shown in Fig. 2(a), with the Fourier transform of the line-out shown in Fig. 2(b). The timing of the peak $|t_{\rm sep}|$ of the side-band determines the separation of the two pulse envelopes.

Figure 2(c) displays a waterfall plot of the spectral line-outs of over 800 successive acquisition shots, obtained during four scans. Scan 1: capillary inserted, laser arriving at start of discharge pulse (laser timing of +30 ns, negligible ionization), pressure scan in 5-shot steps, see inset (d). Scan 2: capillary inserted, laser arriving at the peak of the discharge pulse (laser timing of +300 ns), pressure scan in 5-shot steps, see inset (e). Scan 3: laser timing scan in 10-shot steps. Scan 3 was performed at a fill pressure of 40 Torr. Scan 4: capillary removed from the laser path for 30 shots. The Fourier transform of the spectral line-out delivers the normalized pulse separation $\Delta z_{\rm gr}$ for each of the 800 shots, see Fig. 3(a). Each spectral line-out is also fitted with Eq. (5) to obtain $\phi_{\rm mod}$, and thus Δz_ϕ, see Fig. 3(b). Note that using Eq. (8), Δz_ϕ and $\Delta z_{\rm gr}$ can be converted into plasma density-length products. In terms of diagnostic sensitivity, Scan 4 is relevant since without plasma structure the variation in retrieved Δz reflects the intrinsic single-shot accuracy. The standard deviations σ are found to be $\sigma(\Delta z_{\rm gr})$ =181 nm and $\sigma(\Delta z_\phi) = 4.0$ nm, equivalent to a density-length diagnostic accuracy of $8.2 \cdot 10^{16}$ cm^{-2} from $\Delta z_{\rm gr}$ and $1.8 \cdot 10^{15}$ cm^{-2} from Δz_ϕ. The $\times 45$ lesser sensitivity in $\Delta z_{\rm gr}$ is likely related to small fluctuations in the pulse's longitudinal envelope profile (which is constructed by the spectral phase and intensity over the full spectral bandwidth), whereas determination of Δz_ϕ (from $\phi_{\rm mod}$) is dominated by the intense fringe near frequency ω_0 [vertical dashed line in Fig. 2(c)]. This observation will be further investigated. Note that the error on the mean of a sequence of density-length measurements can be further reduced by a factor $\sigma/\sqrt{N}$ for N samples (at N=30 phase velocity samples in Scan 4 for example, $\sigma/\sqrt{N} = 3.3 \cdot 10^{14}$ cm^{-2}).

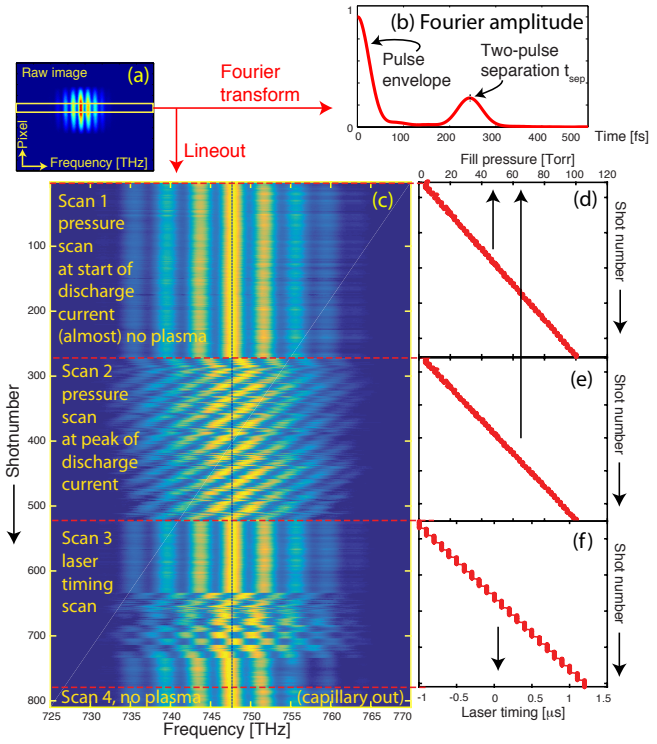

FIG. 2. (color online) (a) Typical single-shot spectral image. (b) Fourier transform of the spectral line-out, delivering the two-pulse separation $t_{\rm sep} = L_{\rm sep}/c$. (c) Waterfall plot of the line-outs obtained in 800 successive shots over four scans. Scan 1: capillary inserted, laser arriving at start of discharge pulse (negligible ionization), pressure scan in 5-shot steps, see inset (d). Scan 2: capillary inserted, laser at peak of discharge pulse (maximum ionization), pressure scan in 5-shot steps, see inset (e). Scan 3: laser timing scan in 10-shot steps, see inset (f). Scan 4: capillary removed, 30 shots.

The pink points of Scan 2 and cyan points of Scan 3 in Fig. 3(b) show that without phase un-wrapping (without adding or subtracting multiples of 2π to adjust the phase), Δz_ϕ simply varies between $-\lambda_0/2$ and $\lambda_0/2$. Accurate phase un-wrapping is not possible when

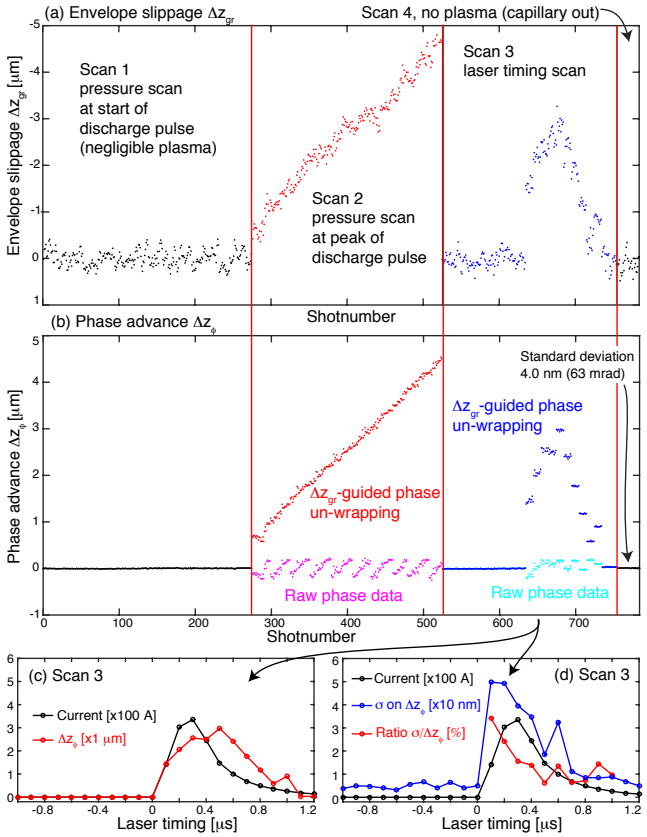

FIG. 3. (color online) From the dataset in Fig. 2(c), the envelope slippage $\Delta z_{\rm gr}$ is plotted in (a) and the phase advance Δz_ϕ in (b), both in units of μm [note that the y-axis is reversed in (a)]. Phase un-wrapping was not applied to the pink points in Scan 2 and cyan points in Scan 3. However, using the simultaneously-obtained $\Delta z_{\rm gr}$ data as a guide, phase tracking was applied resulting in the red points in Scan 2 and blue points in Scan 3. Fig. 3(c) shows for Scan 3 the averaged (over 10 successive points) Δz_ϕ overlapped with the discharge current at each laser timing, whereas (d) show both the standard deviation σ on Δz_ϕ in both absolute (blue, units of [10 nm]) and relative (red, $\sigma/\Delta z_\phi$ in [%]) terms.

the phase jumps more than 2π between successive parameters, which is the case in Scan 2 for the first few data points and in Scan 3 for most points at non-zero current. However, by using the lesser-sensitive group-velocity-based $\Delta z_{\rm gr}$ as a guide (using the knowledge that in a plasma $\Delta z_{\rm gr} = -\Delta z_\phi$), phase tracking was successfully employed. This is demonstrated by the red points of Scan 2 and blue points of Scan 3 in Fig. 3(b). This dataset enabled tracking-free phase correction because the error on the mean $\sigma(\Delta z_{\rm gr})/\sqrt{N}$ for each scan parameter was less than $\lambda_0/2$. Thus, the necessity of tracking from zero-density (slowly ramping up the density from zero to the target value, always maintaining a $< 2\pi$ phase shift) was avoided. For Scan 3, Fig. 3(c) shows the 10-shot-averaged Δz_ϕ points, overlapped with the discharge current at each laser timing. The standard deviation σ on Δz_ϕ is shown in Fig. 3(d) in both absolute (blue, units of [10 nm]) and relative (red, $\sigma/\Delta z_\phi$ in [%]) terms. One can observe that the fluctuations in density-length product drop from $> 3\%$ on the rising edge and peak of the discharge pulse, to $\sim 1\%$ at > 0.3 μs timing. Such observations were not accessible with previous techniques.

In conclusion, we have developed and demonstrated an *in-situ* technique to simultaneously record the phase advance and envelope slippage of probe lasers in a discharged plasma structure. This was accomplished by recording the modulated spectrum of two broad-bandwidth laser pulses in a common-path non-linear interferometer, yielding the line-integrated plasma density. By focusing on both the envelope slippage (periodicity of the spectral modulation) and the phase advance (phase of the modulation), the density-length product was recorded at high-sensitivity without need for phase tracking. The single-shot sensitivity of the diagnostic, measured with the plasma structure removed, was demonstrated to be $\sigma(\Delta z_\phi)$ =4.0 nm, which is equivalent to a density-length product sensitivity of $1.8 \cdot 10^{15}$ cm^{-2}. Multi-shot averaging further reduces the error on the measurement. With the 1.5-cm-long plasma structure inserted, $\Delta z_\phi = -\Delta z_{\rm gr} = 3$ μm was measured at 40 Torr and optimum laser timing, equivalent to a density-length product of $1.4 \cdot 10^{18}$ cm^{-2}. The standard deviation of $8.6 \cdot 10^{15}$ cm^{-2} in this measurement was above the diagnostic sensitivity, thus exposing actual single-shot density-length fluctuations.

ACKNOWLEDGMENTS

This work was supported by the U.S. Department of Energy (DOE) under Contract No. DE-AC02-05CH11231, by the National Science Foundation under Grant No. PHY-1632796, and by the Gordon & Betty Moore Foundation under Grant ID GBMF4898.

[1] E. Esarey, C. B. Schroeder, and W. P. Leemans, Rev. Mod. Phys. **81**, 1229 (2009).
[2] W. P. Leemans, B. Nagler, A. J. Gonsalves, C. Tóth, K. Nakamura, C. G. R. Geddes, E. Esarey, C. B. Schroeder, and S. M. Hooker, Nature Phys. **2**, 696 (2006).
[3] S. Karsch, J. Osterhoff, A. Popp, T. P. Rowlands-Rees, Z. Major, M. Fuchs, B. Marx, R. Hörlein, K. Schmid, L. Veisz, *et al.*, New J. Phys. **9**(11), 415 (2007).
[4] M. Litos, E. Adli, W. An, C. I. Clarke, C. E. Clayton, S. Corde, J. P. Delahaye, R. J. England, A. S. Fisher, J. Frederico, *et al.*, Nature **515**, 92 (2014).
[5] W. K. H. Panofsky and W. R. Baker, Rev. Sci. Instrum. **21**, 445 (1950).
[6] J. van Tilborg, S. Steinke, C. G. R. Geddes, N. H. Matlis,

B. S. Shaw, A. J. Gonsalves, J. V. Huijts, K. Nakamura, J. Daniels, C. B. Schroeder, *et al.*, Phys. Rev. Lett. **115**, 184802 (2015).

[7] A. Butler, A. J. Gonsalves, C. McKenna, D. J. Spence, S. Hooker, S. Sebban, T. Mocek, I. Bettaibi, and B. Cros, Phys. Rev. Lett. **91**, 205001 (2003).

[8] D. M. Gaudiosi, B. Reagan, T. Popmintchev, M. Grisham, M. Berrill, O. Cohen, B. C. Walker, M. M. Murnane, H. C. Kapteyn, and J. J. Rocca, Phys. Rev. Lett. **96**(20), 203001 (2006).

[9] D. J. Spence and S. M. Hooker, Phys. Rev. E **63**(1), 015401 (2000).

[10] A. Butler, D. J. Spence, and S. M. Hooker, Phys. Rev. Lett. **89**(18), 185003 (2002).

[11] C. McGuffey, M. Levin, T. Matsuoka, V. Chvykov, G. Kalintchenko, P. Rousseau, V. Yanovsky, A. Zigler, A. Maksimchuk, and K. Krushelnick, Phys. Plasmas **16**, 113105 (2009).

[12] H. M. Milchberg, T. R. Clark, C. G. Durfee III, T. M. Antonsen, Jr., and P. Mora, Phys. Plasmas **3**(5), 2149 (1996).

[13] J. van Tilborg, S. K. Barber, C. Benedetti, C. B. Schroeder, F. Isono, H.-E. Tsai, C. G. R. Geddes, and W. P. Leemans, Phys. Plasmas **25**, 056702 (2018).

[14] A. J. Gonsalves, T. P. Rowlands-Rees, B. H. P. Broks, J. J. A. M. van der Mullen, and S. M. Hooker, Phys. Rev. Lett. **98**(2), 025002 (2007).

[15] J. van Tilborg, A. J. Gonsalves, E. H. Esarey, C. B. Schroeder, and W. P. Leemans, Opt. Lett. **43**, 2776 (2018).

[16] J. van Tilborg, J. Daniels, A. J. Gonsalves, C. B. Schroeder, E. Esarey, and W. P. Leemans, Phys. Rev. E **89**, 063103 (2014).

[17] J. Daniels, J. van Tilborg, A. J. Gonsalves, C. B. Schroeder, C. Benedetti, E. Esarey, and W. P. Leemans, Phys. Plasmas **22**, 073112 (2015).

[18] F. A. Hopf, A. Tomita, and G. Al-Jumaily, Opt. Lett. **5**(9), 386 (1980).

[19] S. P. Velsko and D. Eimerl, Appl. Opt. **25**(8), 1344 (1986).

[20] P. Burdack, M. Tröbs, M. Hunnekuhl, C. Fallnich, and I. Freitag, Opt. Express **12**(4), 644 (2004).

[21] P. A. Bagryansky, A. D. Khilchenko, A. N. Kvashnin, A. A. Lizunov, R. V. Voskoboynikov, A. L. Solomakhin, H. R. Koslowski, and T. team, Rev. Sci. Instrum. **77**, 053501 (2006).

[22] Y. Hori, T. Yasui, and T. Araki, Optical Review **13**(1), 29 (2006).

[23] F. Brandi and F. Giammanco, Opt. Express **19**(25), 25479 (2011).

[24] T. Akiyama, R. Yasuhara, K. Kawahata, S. Okajima, and K. Nakayama, Rev. Sci. Instrum. **85**, 11D301 (2014).

[25] F. Brandi, F. Giammanco, F. Conti, F. Sylla, G. Lambert, and L. A. Gizzi, Rev. Sci. Instrum. **87**, 086103 (2016).

[26] P. T. Wilson, Y. Jiang, O. A. Aktsipetrov, E. D. Mishina, and M. C. Downer, Opt. Lett. **24**(7), 496 (1999).

[27] C. B. Schroeder, C. Benedetti, E. Esarey, J. van Tilborg, and W. P. Leemans, Phys. Plasmas **18**, 083103 (2011).